

# Machine learning-enabled camera free speckle wavemeter

TIANLIANG WANG, YI LI,<sup>\*</sup> XINYU GAO, JINCHAO TAO, XU WANG, QIN LIANG, YANQING QIU, BANGNING MAO, AND YANLONG MENG

*College of Optical and Electronic Technology, China Jiliang University, Hangzhou 310018, China*

*\*yli@cjlu.edu.cn*

## Abstract:

Recovering the wavelength from disordered speckle patterns has become an exciting prospect as a wavelength measurement method due to its high resolution and simple design. In previous studies, panel cameras have been used to detect the subtle differences between speckle patterns. However, the volume, bandwidth, sensitivity, and cost (in non-visible bands) associated with panel cameras have hindered their utility in broader applications, especially in high speed and low-cost measurements. In this work, we broke the limitations imposed by panel cameras by using a quadrant detector (QD) to capture the speckle images. In the scheme of QD detection, speckle images are directly filtered by convolution, where the kernel is equal to one quarter of a speckle pattern. First, we proposed an up-sampling algorithm to pre-process the QD data. Then a new convolution neural network (CNN) based algorithm, shallow residual network (SRN), was proposed to train the up-sampled images. The experimental results show that a resolution of 4 fm ( $\sim 0.5$  MHz) was achieved at 1550nm with an updating speed of  $\sim 1$  kHz. More importantly, the SRN shows excellent robustness. The wavelength can be precisely reconstructed from raw QD data without any averaging, even where there exists apparent noise. The low-cost, simple structure, high speed and robustness of this design promote the speckle-based wavemeter to the industrial grade. In addition, without the restriction of panel cameras, it is believed that this wavemeter opens new routes in many other fields, such as distributed optical fiber sensors, optical communications, and laser frequency stabilization.

## Introduction

The measurement of laser wavelength plays a crucial role in the application of optical sensors, communications, fluorescence spectroscopy, and metrology [1-6]. Traditional wavemeters are mainly based on the Michelson, Fizeau, and Fabry–Perot interferometers [7-9]. However, due to their large volume and low measurement speed, they are not well suited for complex environments. Many researchers of laser speckles have found that the speckles contain wavelength information, thus providing a new way to design a more compact and higher resolution wavemeter [10-13]. When coherent light is incident on a random media (such as rough surface or disordered diffuser), numerous distinct granular speckles can be easily observed via a panel camera [14,15]. At the beginning, these speckles were used to measure fluid velocity, surface morphology [16], and blood flow [17,18]. Goodman first pointed out that the intrinsic nature of speckles is related to the light frequency [14]. Subsequent researchers found that edges of the speckles appear to change randomly when the wavelength slightly varies [19]. Cao was first to report an all-fiber spectrometer based on the laser speckles [20]. A 5m long multimode fiber was used as the light diffuser media and a monochrome InGaAs camera was used as the speckle acquisition device. By using the transmission matrix algorithm (TMA) [21,22], the spectrometer achieved a resolution of 0.03 nm. Additionally, a high-resolution wavemeter based on a fiber-coupled integrating sphere

was demonstrated [6]. In this research, the speckle patterns were captured by a CMOS camera. The algorithm of principal component analysis (PCA) enabled sub-femtometer wavelength resolution. In another paper, a high-resolution spectrometer with large bandwidth was reported, which used an optical fiber taper as the speckle generator [23]. The resolutions were 40 pm and 10 pm in the visible and infrared range, respectively. Derek M. Kita reported a speckle-based Fourier spectrometer [24], where the camera and the designed waveguide were integrated together. By using an optimized TMA, the device has a resolution of 140 MHz with a bandwidth of 12 nm. In our previous work, a 1-meter long RCF (Rectangular core fiber) was used as the diffuser and polarization modulated speckles were captured by an InGaAs camera, achieving a final resolution of 0.2 femtometers [25]. Extracting the differences of speckle patterns at different wavelengths is the key point of the speckle wavemeter. However, the image differences are usually very subtle, especially among the speckle patterns with smaller wavelength differences. In addition, the changes in the speckle patterns occur throughout the entire optical field and appear to be totally disordered. These changes have not been predicted by any theory previously. Therefore, in the above studies, panel cameras are no doubt the most suitable tool to record the entire speckle pattern and completely capture its fine details. However, using a camera also brings some shortcomings. Limited by exposure time, cameras are unable to satisfy the requirement of high-speed measurement in applications such as laser frequency stabilization [6,26,27], optical fiber distributed sensors[28], and optical fiber communications[1,29]. Large amounts of image data are also a heavy burden to the computational consumption associated with data transmission, image processing, and wavelength reconstruction. And panel cameras, with exception to those which operate in the visible spectrum, are extremely expensive, for instance near infrared InGaAs cameras, which limit the feasibility of panel cameras in the non-visible range.

It is well known that many images can be sparsely represented [30]. Thus, the image information can be acquired using very few detectors if the valid information is of low dimension, which has previously been used in the construction of CT images and single photo detector imaging [31,32]. In the case of speckles, the speckle data is over redundant if it is desired to measure only the wavelength. So, it should be possible to use substantially fewer photo detectors to obtain the wavelength information. However, using few detectors will create difficulties when using current reconstruction algorithms, such as TMA and PCA. Because the building of the transmission matrix algorithm (TMA) and the extraction of the principal components analysis (PCA) rely on thousands of pixels, few data input will be an extremely ill-posed problem for them. Additionally, pixel noise such as shot noise, will lower the reliability of the reconstruction accuracy as the noise cannot be effectively identified by these algorithms.

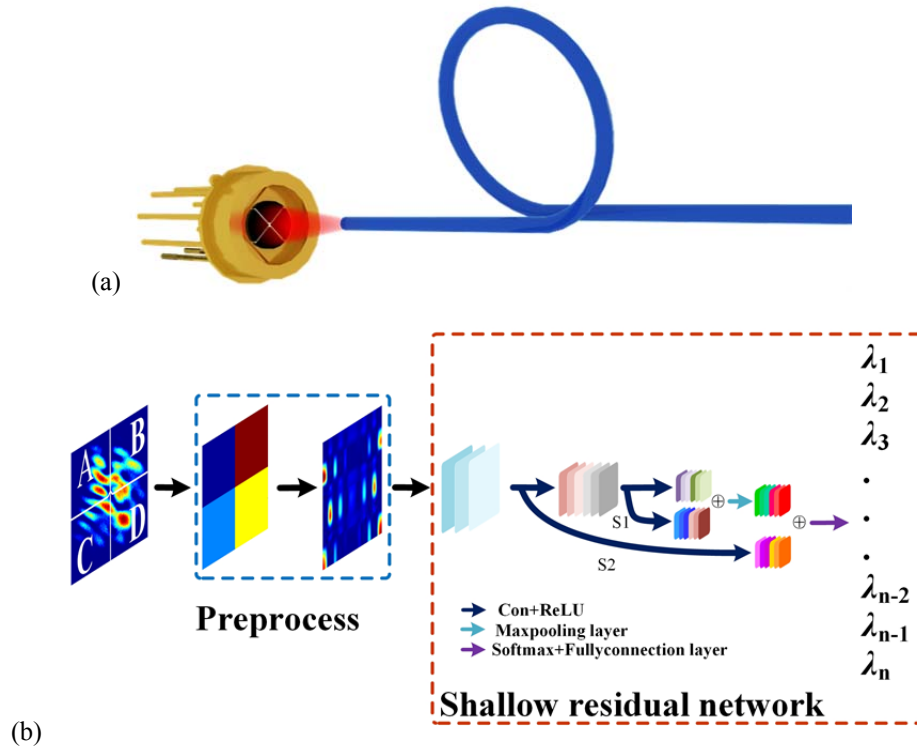
In this study, a camera free speckle wavemeter was proposed and demonstrated by using a quadrant detector (QD). It breaks through the physical limitations brought by using a panel camera and paves a new way to design a compact, low-cost and high-speed wavemeter. The QD can be regarded as four independent detectors, each one detecting one quadrant of the speckle pattern. Compared with the CCD or COMS, the independent detector has the advantage of low-cost, large dynamic range and high bandwidth. To adapt the new wavemeter design, a machine learning based algorithm, Shallow Residual Network (SRN), was firstly proposed. The experimental results have shown that the wavelength resolution is 4 fm ( $\sim$  0.5 MHz) around 1550nm. More importantly, SRN shows strong robustness and high efficiency, which allows for the fastest and most real-time measurement possible.

## **Results**

### *Experimental setup*

QD is usually applied in light spot detection due to its high sensitivity to lateral movements. It splits the detection area into 4 independent parts, each taking one quadrant of the circular light receiving area, so named as quadrant detector. In this work, a QD (HAMAMASTU G6849, spectral response range from 0.9 to 1.7  $\mu\text{m}$ , cutoff frequency = 30 MHz) was used as the photo detector. A 50 cm long RCF (NA = 0.15, outer diameter = 125  $\mu\text{m}$ , core = 100  $\times$  25  $\mu\text{m}$ ) was utilized as the diffusing media. And a polarization maintaining fiber (PMF) was connected to the RCF to avoid polarization disturbance. In order to eliminate noise produced from ambient light and environmental vibrations, the detector and the RCF were fixed together using a funnel-shaped mold. The schematic diagram and wavelength reconstruction algorithm of this wavemeter are shown in figure 1(a) and (b). Four low-noise high-precision operational amplifiers were used to amplify the output currents and to convert them into analog signals. Then, the signals were sampled by a data acquisition card (National Instrument USB-6251, acquisition depth = 16 bit). Benefiting from higher acquisition depth, the QD can detect more subtle intensity changes compared with panel cameras which are only of 8~12 bit.

As shown in Figure 1 (c), the speckle pattern was divided into four parts (A, B, C, D) in the QD detection. So the speckle image was compressed into just four intensities. When tuning the wavelength of the input light, the intensity distribution of the speckle pattern varies due to the mode interference in the multimode fiber and the QD data is consequently changed. Figure 1 (d) shows intensity variations of the QD in the range of 1530 nm -1563 nm with a step of 5 pm. It can be seen that the intensity of each channel is strong wavelength dependent.



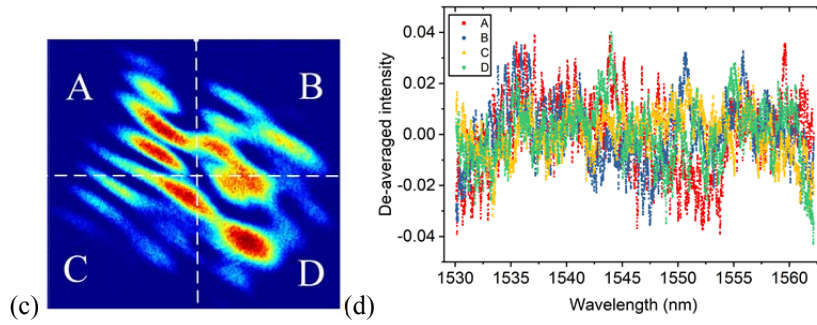


Figure 1 (a) Schematic diagram of the wavemeter. (b) Brief architecture of the SRN. (c) The speckle pattern of the RCF detected by a QD. (d) The recorded intensity of the QD in the range of 1530-1562 nm.

### Up-sampling algorithm

As mentioned above, the largest challenge in this work is extracting the wavelength information from only four quadrants of data. In the scheme of quadrant detection, the speckle patterns were lossily compressed to four independent outputs as shown in the figure 1(b). The four photo intensities were saved as a  $2 \times 2$  matrix. As shown in the figure 2, an up-sampling is then utilized to expand the original matrix from  $2 \times 2$  to  $100 \times 100$  to maximize the difference between patterns and improve the resolution. The up-sampling includes two steps, power coding and bicubic interpolation. After the four original intensities were normalized, their 1st to 144th powers were calculated using a step of four. As shown in Equation 1, the powered intensities were coded and reshaped to the  $12 \times 12$  matrix,  $A_c$ .  $A_c$  is then the coded matrix (figure 2 (b)), while sixteen identical  $1 \times 4$  raw data arrays form  $A_o$ . This operation can enrich the distribution of the data characteristics and improve the signal-to-noise ratio.

$$A_{c,12 \times 12} = A_{o,12 \times 12} P_{2 \times 12} = \begin{bmatrix} A_{1 \times 4} & A_{1 \times 4}^{144} & A_{1 \times 4}^9 \\ A_{1 \times 4}^{17} & A_{1 \times 4}^{125} & A_{1 \times 4}^{25} \\ \vdots & \cdots & \vdots \\ A_{1 \times 4}^{121} & A_{1 \times 4}^{21} & A_{1 \times 4}^{129} \\ A_{1 \times 4}^{13} & A_{1 \times 4}^{137} & A_{1 \times 4}^5 \end{bmatrix}_{12 \times 12} \quad (1)$$

After the quadrant data is coded by power, the bicubic interpolation is subsequently applied to further increase the matrix to  $100 \times 100$ . In bicubic interpolation, a point is interpolated by the gray values of the 16 neighboring points around it ( $4 \times 4$ ) [33]. The final up-sampled image is shown in figure 2(c).

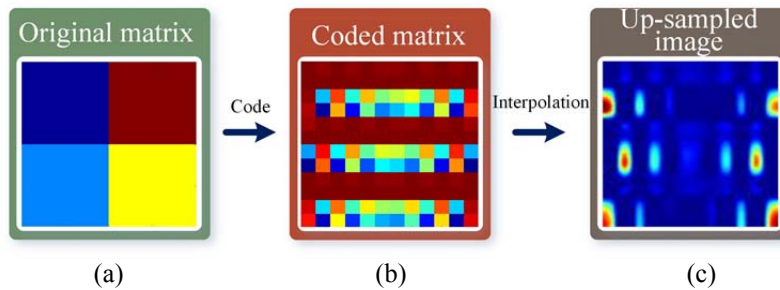


Figure 2 (a) The original data of a determined wavelength. (b) The coded data of the original data. (c) The final up-sampled image.

### Design of the Shallow Residual Network (SRN)

Machine learning algorithms were then applied to reconstruct the wavelength. A CNN based algorithm, Alexnet, was used first and its classification accuracy was found to be  $\sim 93\%$ . We noted that a highly accurate image classification was reported by using the Deep Residual Network (DRN) in ref. [33]. The high accuracy was mainly attributable to the multiple residual blocks (RB) in the network. RB makes the network deeper and more accurate without adding extra parameters and computational complexity [34-37]. As shown in figure 3, the strategy of the RB is to add a shortcut connection (SC) between the input and output of the stacked nonlinear layers. This changes the mapping of the stacked layers to residual mapping [34]. Inspired by the DRN, we reformed Alexnet as follows to boost its accuracy. Two SCs, S1, S2, shown in figure 1 (b), were added to the original Alexnet structure and a fully connected layer of Alexnet was replaced by a max pooling layer. The reformed network only has two RBs in this work, so called shallow residual network (SRN) (see supplement document for more details of the SRN). Through the short connections and down sampling operations, the network captures more wavelength related features and can classify the images with higher accuracy.

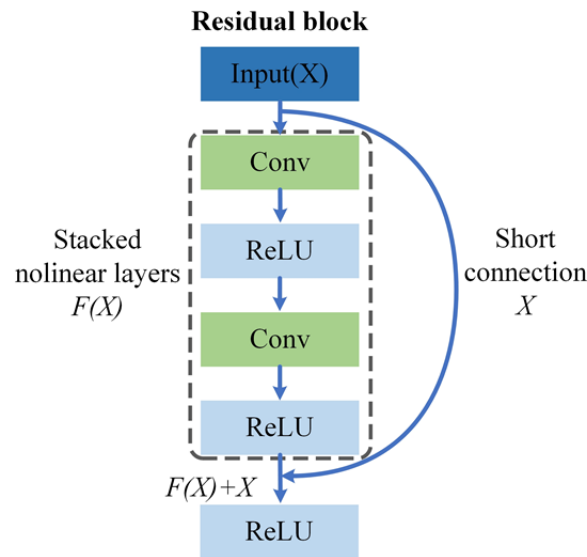


Figure 3 The framework of the residual block. The RB consists of several convolution layers (Conv) and activation layers (ReLU). Suppose there is no short connection in the RB. The mapping of the stacked nonlinear layers is  $F(X)$ , the desired output of these layers is  $Y$ , thus we have  $F(X) = Y$ . The training processing can be considered as fitting  $X$  to  $Y$  through mapping function  $F$ . However, when adding a short connection into the RB network, the desired output is changed to  $F(X)+X$ , renamed as  $H(X)$ . The fitting process of the stacked nonlinear layers are then changed to  $F(X)=H(X)-X$ . For most cases, the residual mapping is much easier to optimize than the original mapping [34]. RB makes the network deeper and more accurate, without adding the extra parameters and computational complexity.

### Wavelength measurement accuracy

The training progress is displayed in figure 4 (a), which shows the accuracy (blue dot) and loss (red dot) of the validation dataset. It can be seen that as the number of iterations increases, the loss and accuracy approach 0 and 100 respectively. After about 3400 iterations, the slope

of each curve becomes gradual. The results show that the accuracy and loss of our network after 17000 iterations are 100% and  $\sim 0.0004$  respectively. Additionally, the accuracy of the network was examined using selected test images (24 pieces per wavelength). The wavelengths of the test set are known but have never been trained. The classification results from the network are displayed in a confusion chart, as shown in figure 4 (b). The chart can be regarded as a matrix, where the rows and the columns represent the predicted wavelengths and the true wavelengths respectively. Diagonal elements correspond to correctly classified wavelengths while off-diagonal elements correspond to incorrectly classified wavelengths. The values of the diagonal element denote the number of correctly classified pieces for each tested wavelength. All the test results show that the resolution of the wavemeter is better than 0.5 MHz ( $\sim 4$  fm) (The laser modulation system and the training options can be seen in the methods section).

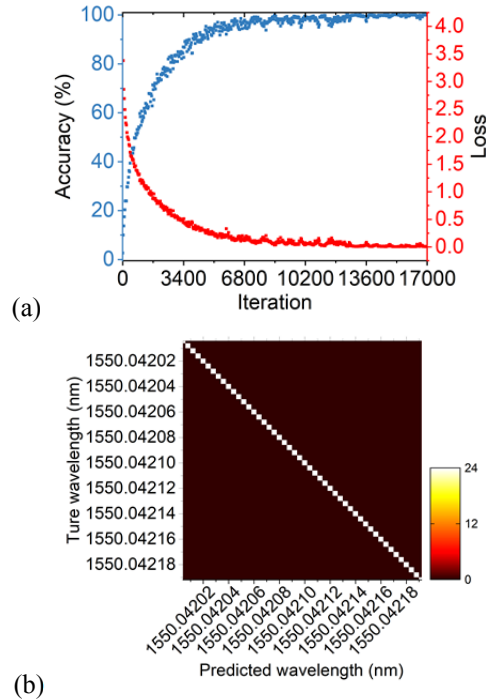


Figure 4 (a) The accuracy and loss of the validation dataset during training. (b) The result of the wavelength classification using a trained network. The intensity of the diagonal elements represents the number of the images predicted in each wavelength which illustrates the accuracy of the trained network.

### Comparison of different wavelength reconstruction algorithms

Different wavelength reconstruction algorithms including SRN, Alexnet [38], VGG16 [39], and Resnet18 [34] were then compared using the same up-sampled dataset (see supplementary document for Alexnet, VGG19, and Resnet18 training details and confusion charts). From Table 1, Alexnet takes the shortest time to complete one classification due to its simple structure, while VGG19 is the slowest algorithm of all the networks because VGG19 has 3 fully connected layers which consume a lot of computing resources. Furthermore, although Resnet18 takes only 0.00092s to recover the wavelength, it only achieves an accuracy of 67.70%. The reformed SRN has distinct advantages over the other networks,

especially in time consumption and accuracy. These advantages arise from a clever network structure and a more suitable allocation of computational resources.

**Table 1. Comparison of different reconstruction algorithms.**

Algorithm	Time (s)	Accuracy
Alexnet	~ 0.00071	~ 93.32%
VGG19	~ 0.00256	~ 94.53%
Resnet18	~ 0.00092	~ 67.70%
SRN	~ 0.00071	100%

To test the high-speed performance of the proposed wavemeter, a real-time measurement system was built as follows. We set the MWS to sweep mode to modulate the laser frequency. The frequency modulation amplitude was 24 MHz, with a repetition frequency of 20 Hz. The data sampling rate was 1000 points per second, corresponding to a 0.5 MHz frequency difference between each sampling point. The original raw data without any averaging is shown in Figure 5 (a). The data was first processed by the method described above and was then sent to the already trained network to extract the wavelength. All the image processing and reconstruction codes were run on a GPU. Part of the classification results are shown in Figure 5 (a). The wavelengths were all identified using SRN with an updating speed of ~ 1kHz. Since the speckle image is acquired by a QD, the data sampling speed is no longer the bottleneck of the measurement. The wavelength measurement speed largely depends on the core number of Compute Unified Device Architectures (CUDA). Parallel computing with multiple graphics cards can greatly increase the speed. It should be noted that the SRN shows excellent robustness and high-speed wavelength recovery simultaneously.

#### *Robustness of the SRN*

As shown in Figure 5 (a), the system noise of the original raw data is enlarged in the side insets. Although the noise looks apparent, the wavelengths are still precisely recovered without any extra processing, such as averaging or filtering. Figure 5 (b) shows two up-sampled images from two measurements at the same wavelength. Some of the speckles' size and intensity distributions are different, an effect which arises from the data noise. However, the noise can be learned in the data training processing, thus the SRN can recognize if the changes are wavelength dependent or not. It is believed that the SRN precisely discriminates the wavelength from not only the image details but from the image structure information [40]. The robustness ensures measurement reliability in a complex environment, which is of great importance for industrial applications.

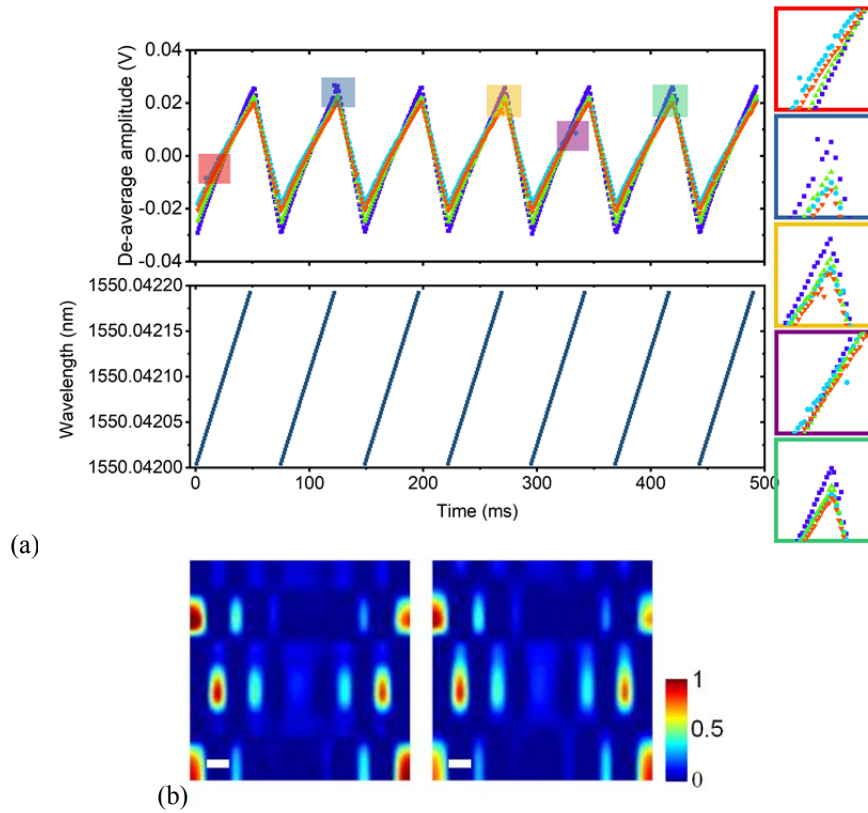


Figure 5 (a) The original raw data set acquired by the QD. The enlarged parts of the data show the system noise. (b) Two up-sampled images with the same wavelength of 1550.04202 nm. Although there exist apparent differences in the two images, the predicted wavelengths coincide with the true wavelength. The inset white scale bar is 10 pixels.

## Discussions

Based on the speckle patterns' highly sensitive dependence on wavelength, many high-resolution wavemeters have been proposed in recent years. Since the speckle patterns are usually disordered, panel cameras have been chosen to record the differences between speckle patterns. Inspired by the compressed sensing used in the acquisition of low-dimensional information, we try to explore performing wavelength measurements from the speckle patterns using only a few detectors. In this study, we utilized a QD to acquire the fiber speckles differences among different wavelengths. Although the QD only has four independent outputs, its large dynamic range (16 bit in this work, can be higher in principle) compensates the shortage of speckle information to a certain extent. Through QD detection, the speckle image was filtered by convolution, where the size of convolution kernel is equal to a quarter of the speckle pattern. In order to maximize the difference between patterns and improve the resolution, the original  $2 \times 2$  QD data was coded by power and finally up-sampled to a  $100 \times 100$  image. A new machine learning algorithm, SRN was proposed to train the pre-processed images. The experimental results show that the wavemeter achieves a resolution of 4 fm with the help of SRN, which exhibits superior performance over other algorithms in terms of accuracy and efficiency, while simultaneously showing excellent robustness to the noise. The QD data can be precisely classified without any averaging, even if there exists apparent noise. Since the SRN relies on the input data, the measurement range of this wavemeter should be within the training dataset. At present, the main factor limiting the speed is the computing power.



In conclusion, this study breaks through the physical limitations imposed by panel cameras and provides a camera free solution in designing compact, low-cost, high-speed and high-resolution wavemeters. These findings should also benefit other applications such as low noise distributed fiber sensors, laser frequency stabilization, and pulsed laser measurements [41-44]. The QD design could be also used to recover broadband spectrum, which will be part of our future study. Furthermore, the device design and signal processing methods in this study can be applied in multi-dimensional optical measurements [45], especially when hardware resources are constrained.

## Methods and materials

### Laser frequency tuning system

A ultra-high precision laser frequency tuning system was built as the light source to test the performance of the SRN. Light from a low noise distributed feedback (DFB) laser (RIO ORION™ Series 1550 nm, with central wavelength of 1550.042 nm and linewidth of 7 kHz) was modulated by an electro-optic modulator (EOM) (iXblue, MPZ-LN-10). The modulation signal was generated by a microwave source (MWS) (HP8341B). A power amplifier (PA) was used to amplify the modulation signal and drive the EOM. Then, the frequency ( $\nu_0$ ) of the DFB laser was modulated by a frequency biases  $\Delta\nu$  into a series of symmetrical sidebands, such as  $\dots, \nu_0 - \Delta\nu, \nu_0, \nu_0 + \Delta\nu \dots$ . By using an optical tunable filter (OTF) (Yenista Optics, XTM-50), only one sideband ( $\nu_0 - \Delta\nu$ ) is preserved. When the frequency of the drive signal changes, the central wavelength of the laser can be quickly modulated. Note that the tuning resolution of this system is limited by the laser linewidth and the precision of the MWS [25,46]. The complete modulation process is shown in figure 6 (a). The central frequency of the DFB laser was finely tuned by  $\nu_{step}$  with the frequency bias ( $\nu_{bias}$ ). This relationship can be expressed by  $\Delta\nu = \nu_{bias} + n \times \nu_{step}$ , where  $\Delta\nu$  is the modulated frequency and  $n$  is the number of tuning channels. The modulated laser frequency with different frequency biases of 6 GHz and 10 GHz can be seen in the supplementary information. The MWS is set to continuous mode, with  $\nu_{bias} = 10$  GHz,  $\nu_{step} = 0.5$  MHz, and  $n = 48$ . The laser frequency is tuned by forty-eight steps (24 MHz) with a frequency switch time of 200ms. The corresponding quadrant data was recorded and up sampled as the original dataset.

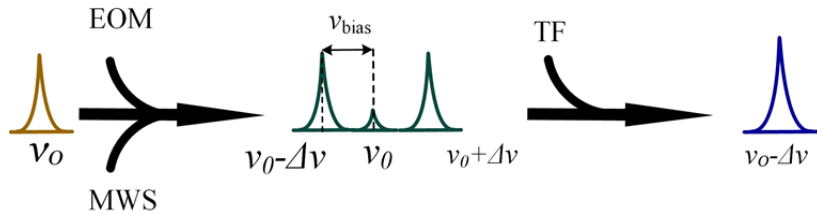


Figure 6 Diagram of the laser frequency modulation.

### Training options and platform

The training set, test set, and validation set accounted for 60%, 20%, 20% of the original dataset respectively. Note that these images in each set were randomly sampled. The training was run on MATLAB through a graphics processing unit (GPU) (Nvidia GeForce GTX 960, 4G). We specified the solver as 'adam' [47] and set the mini-batch size and maximum number of epochs to 48 and 100 respectively. The cross-entropy error function is set as the cost function [48].

### *Acknowledgements*

This work was funded by the Natural Science Foundation of Zhejiang Province (Grant Nos. LY16F050006) and the Zhejiang Provincial Department of Science and Technology (Zhejiang Xinmiao Talents Program) (Grant No. 2020R409042).

### *Competing interests*

The authors declare that they have no competing financial interests.

### *Contributions*

Yi Li and Tianliang Wang designed the wavemeter. Tianliang Wang developed the up-sampling algorithm and the wavelength reconstruction algorithm. Xinyu Gao optimized the algorithms and analyzed the data. Tianliang Wang, Jinchao Tao, Xu Wang, and Yanqing Qiu built the data acquisition and processing system. Tianliang Wang, Jinchao Tao, Qin Liang, Bangning Mao, and Yanlong Meng did the experiments. Tianliang Wang and Yi Li wrote the paper. Yi Li supervised the study.

### *Data availability*

All the data and methods needed to evaluate the conclusions of this work are presented in the main text and the Supplementary Information. Additional data can be requested from the corresponding author.

### *Supplementary information*

See the supplementary material.zip

### **References**

1. Richardson, D. J., J. M. Fini, and Lynn E. Nelson. "Space-division multiplexing in optical fibres." *Nature photonics* 7.5 (2013): 354-362.
2. Greenberg, Aaron P., Gautam Prabhakar, and Siddharth Ramachandran. "High resolution spectral metrology leveraging topologically enhanced optical activity in fibers." *Nature communications* 11.1 (2020): 1-7.
3. Bashan, Gil, et al. "Distributed cladding mode fiber-optic sensor." *Optica* 7.1 (2020): 85-92.
4. Maurice, James, et al. "Transcutaneous fluorescence spectroscopy as a tool for non-invasive monitoring of gut function: first clinical experiences." *Scientific reports* 10.1 (2020): 1-13.
5. Erf, Robert, ed. *Speckle metrology*. Elsevier, 2012.
6. Metzger, Nikolaus Klaus, et al. "Harnessing speckle for a sub-femtometre resolved broadband wavemeter and laser stabilization." *Nature communications* 8 (2017): 15610.
7. Lawall, John, and Ernest Kessler. "Michelson interferometry with 10 pm accuracy." *Review of Scientific Instruments* 71.7 (2000): 2669-2676.
8. Kajava, T. T., H. M. Lauranto, and R. R. E. Salomaa. "Fizeau interferometer in spectral measurements." *JOSA B* 10.11 (1993): 1980-1989.
9. Vaughan, M. *The Fabry-Perot interferometer: history, theory, practice and applications*. Routledge, 2017.
10. Hanson, Steen G., Michael Linde Jakobsen, and Maumita Chakrabarti. "Speckle-based wavemeter." *SPECKLE 2015: VI International Conference on Speckle Metrology*. Vol. 9660. International Society for Optics and Photonics, 2015.
11. Gupta, Roopam K., et al. "Deep learning enabled laser speckle wavemeter with a high dynamic range." *Laser & Photonics Reviews* 14.9 (2020): 2000120.
12. Hornig, G. J., et al. "Wavemeter based on dispersion and speckle in a tapered hollow waveguide." *OSA Continuum* 2.2 (2019): 495-506.
13. Metzger, Nikolaus Klaus, et al. "Integrating sphere based speckle generation for wavelength determination and laser stabilization." *Frontiers in Optics*. Optical Society of America, 2016.
14. Goodman, Joseph W. *Speckle phenomena in optics: theory and applications*. Roberts and Company Publishers, 2007.
15. Rahmani, Babak, et al. "Actor neural networks for the robust control of partially measured nonlinear systems showcased for image propagation through diffuse media." *Nature Machine Intelligence* 2.7 (2020): 403-410.

16. Cheng, Chuanfu, et al. "Absolute measurement of roughness and lateral-correlation length of random surfaces by use of the simplified model of image-speckle contrast." *Applied optics* 41.20 (2002): 4148-4156.
17. D. B. Barker and M. E. Fourney, "Measuring fluid velocities with speckle patterns," *Opt. Lett.* 1, 135–137 (1977).
18. Zhou, Wenjun, et al. "Highly parallel, interferometric diffusing wave spectroscopy for monitoring cerebral blood flow dynamics." *Optica* 5.5 (2018): 518-527.
19. Bruce, Graham D., et al. "Overcoming the speckle correlation limit to achieve a fiber wavemeter with attometer resolution." *Optics letters* 44.6 (2019): 1367-1370.
20. Redding, Brandon, and Hui Cao. "Using a multimode fiber as a high-resolution, low-loss spectrometer." *Optics letters* 37.16 (2012): 3384-3386.
21. Redding, Brandon, et al. "Compact spectrometer based on a disordered photonic chip." *Nature Photonics* 7.9 (2013): 746-751.
22. Redding, Brandon, et al. "High-resolution and broadband all-fiber spectrometers." *Optica* 1.3 (2014): 175-180.
23. N. H. Wan, F. Meng, T. Schröder, R.-J. Shiue, E. H. Chen, and D. Englund, "High-resolution optical spectroscopy using multimode interference in a compact tapered fibre," *Nat. Commun.* 6, 7762 (2015).
24. Paudel, Uttam, and Todd Rose. "Ultra-high resolution and broadband chip-scale speckle enhanced Fourier-transform spectrometer." *Optics Express* 28.11 (2020): 16469-16485.
25. Wang, Tianliang, et al. "High-resolution wavemeter based on polarization modulation of fiber speckles." *APL Photonics* 5.12 (2020): 126101.
26. Olson, Judith, et al. "Ramsey-bordé matter-wave interferometry for laser frequency stabilization at 10– 16 frequency instability and below." *Physical review letters* 123.7 (2019): 073202.
27. Coluccelli, Nicola, et al. "The optical frequency comb fibre spectrometer." *Nature communications* 7.1 (2016): 1-11.
28. Murray, Matthew J., et al. "Speckle-based strain sensing in multimode fiber." *Optics express* 27.20 (2019): 28494-28506.
29. Keiser, Gerd. "Optical fiber communications." *Wiley encyclopedia of telecommunications* (2003).
30. Candès, ETMAnuel J., and Michael B. Wakin. "An introduction to compressive sampling." *IEEE signal processing magazine* 25.2 (2008): 21-30.
31. Cabral, Thales Wulfert, et al. "Compressive sensing in medical signal processing and imaging systems." *Sensors for Health Monitoring*. Academic Press, 2019. 69-92.
32. Turpin, Alex, et al. "Spatial images from temporal data." *Optica* 7.8 (2020): 900-905.
33. Keys, Robert. "Cubic convolution interpolation for digital image processing." *IEEE transactions on acoustics, speech, and signal processing* 29.6 (1981): 1153-1160.
34. He, Kaiming, et al. "Deep residual learning for image recognition." *Proceedings of the IEEE conference on computer vision and pattern recognition*. 2016.
35. Targ, Sasha, Diogo Almeida, and Kevin Lyman. "Resnet in resnet: Generalizing residual architectures." *arXiv preprint arXiv:1603.08029* (2016).
36. Wu, Zifeng, Chunhua Shen, and Anton Van Den Hengel. "Wider or deeper: Revisiting the resnet model for visual recognition." *Pattern Recognition* 90 (2019): 119-133.
37. Szegedy, Christian, et al. "Inception-v4, inception-resnet and the impact of residual connections on learning." *arXiv preprint arXiv:1602.07261* (2016).
38. Krizhevsky, Alex, Ilya Sutskever, and Geoffrey E. Hinton. "Imagenet classification with deep convolutional neural networks." *Communications of the ACM* 60.6 (2017): 84-90.
39. Simonyan, Karen, and Andrew Zisserman. "Very deep convolutional networks for large-scale image recognition." *arXiv preprint arXiv:1409.1556* (2014).
40. Helgadottir, Saga, Aykut Argun, and Giovanni Volpe. "Digital video microscopy enhanced by deep learning." *Optica* 6.4 (2019): 506-513.
41. Murray, Matthew J., and Brandon Redding. "Quantitative strain sensing in a multimode fiber using dual frequency speckle pattern tracking." *Optics Letters* 45.6 (2020): 1309-1312.
42. Benabid, Fetah, et al. "Compact, stable and efficient all-fibre gas cells using hollow-core photonic crystal fibres." *Nature* 434.7032 (2005): 488-491.
43. Xiong, Wen, et al. "Multimode-fiber-based single-shot full-field measurement of optical pulses." *Optics Letters* 45.8 (2020): 2462-2465.
44. Xiong, Wen, et al. "Deep learning of ultrafast pulses with a multimode fiber." *APL Photonics* 5.9 (2020): 096106.
45. Cui, Qi, et al. "Snapshot hyperspectral light field imaging using image mapping spectrometry." *Optics Letters* 45.3 (2020): 772-775.
46. Zhang, Yixin, et al. "High-Resolution Sensing System Based on Fiber Bragg Grating Fabry–Perot Interferometer and Frequency-Domain Demodulation." *IEEE Sensors Journal* 19.12 (2019): 4451-4457.
47. Kingma, Diederik P., and Jimmy Ba. "Adam: A method for stochastic optimization." *arXiv preprint arXiv:1412.6980* (2014).
48. Kline, Douglas M., and Victor L. Berardi. "Revisiting squared-error and cross-entropy functions for training neural network classifiers." *Neural Computing & Applications* 14.4 (2005): 310-318.